Journal of Science and Transport Technology
Journal homepage: https://jstt.vn/index.php/en

# Interpolating Modified Moving Least Squares-based meshless method for large deformation analysis in hyperelastic model

Kha Vy Vu Hoang[1,2], Thanh Trung Nguyen[3], Hai Nhan Le[4], Xuan Dai Le[1,2], Nha Thanh Nguyen[1,2,*]

[1]Department of Engineering Mechanics, Faculty of Applied Science, Ho Chi Minh City University of Technology (HCMUT), 268 Ly Thuong Kiet Street, Dien Hong Ward, Ho Chi Minh City, Vietnam

[2]Vietnam National University Ho Chi Minh City, Linh Xuan Ward, Ho Chi Minh City, Vietnam

[3]TechnoStar Co. Ltd, Tokyo, Japan

[4]School of Mechanical and Mining Engineering, The University of Queensland, Brisbane, QLD 4072, Australia

**Article info**
**Type of article:**
Original research paper

**DOI:**
https://doi.org/10.58845/jstt.utt.2026.en.6.2.375-387

***Corresponding author:**
Email address:
nhanguyen@hcmut.edu.vn

**Received:** 07/12/2025
**Received in Revised Form:** 24/04/2026
**Accepted:** 27/05/2026

**Abstract:** This work develops a meshfree interpolation approach based on the Interpolating Modified Moving Least Squares (IMMLS) approximation for the accurate simulation of hyperelastic materials undergoing large deformations. As an enhanced interpolation technique within the family of Element-Free Galerkin (EFG)-type methods, IMMLS provides a flexible numerical framework for problems in which conventional mesh-based approaches often encounter difficulties under severe deformation. Since hyperelastic materials are characterized by highly nonlinear constitutive behavior and can sustain large strains, their response is most appropriately described within the framework of finite deformation theory, making an accurate treatment of such nonlinearity essential for reliable numerical modelling. To assess the capability of the proposed method, the Neo-Hookean model was adopted as a representative constitutive model for large-deformation analysis, while the material parameters were selected from existing literature to ensure consistency and accuracy. The numerical results were compared with reference data reported in previous studies, and the computational implementation was further validated against benchmark solutions obtained in MATLAB. In addition, the broader engineering relevance of the IMMLS approach is discussed through its potential applications, and the present findings are expected to provide a useful basis for future, more detailed investigations in this field.

**Keywords:** Meshless method, Interpolating Modified Moving Least Squares, hyperelastic model, large deformation.

## 1. Introduction

Mechanics of hyperelastic materials, which require large deformation analysis, plays an essential role in various fields, ranging from material science and polymer engineering (e.g., rubber, elastomeric components, foams and gels, and shape memory polymers), mechanical and automotive engineering (e.g., flexible joints and couplings, tire modeling, and soft robotics), to biomedical engineering (e.g., soft tissue modeling,

biomechanical analysis of organs, and textile and wearable technologies) [1]. When hyperelastic constitutive laws are combined with near-incompressibility characteristics, classical numerical methods may suffer significantly from volumetric locking in standard finite element formulations [2, 3]. Furthermore, finite element meshes tend to distort severely under large strains, leading to loss of accuracy or even computational failure when elements become excessively deformed [4]. Mixed displacement-pressure elements have been introduced to alleviate locking [3], while frequent remeshing has also been employed to overcome mesh distortion. However, these treatments bring additional challenges, such as increased computational cost and possible degradation of solution fidelity [5].

As a promising alternative for the analysis of hyperelastic structures, meshfree methods bypass fixed element connectivity and predefined meshes. For example, the Element-Free Galerkin (EFG) method represents the computational domain by a set of nodes, thereby enabling more straightforward treatment of large deformations and material separation without the mesh entanglement issues typically encountered in FEM [6, 7]. In particular, meshfree EFG methods inherently avoid mesh-distortion problems during extreme deformations and have demonstrated robust performance in scenarios such as crack propagation and soft tissue simulation, where conventional FEM would require complex remeshing procedures [7, 8]. Besides the classical EFG formulation, other meshfree approaches, such as reproducing kernel particle methods and related Galerkin-free schemes, have also been developed for nonlinear and large-deformation analysis [9-11]. Moreover, stabilized nodal integration techniques and general review studies have further enriched the development and robustness of meshfree methods in computational solid mechanics [12, 13]. On the other hand, the lack of the Kronecker-delta property, which complicates the direct imposition of essential (Dirichlet) boundary conditions, remains a major drawback of conventional EFG formulations based on Moving Least Squares shape functions [14].

Recent advances have addressed this limitation of conventional meshfree methods by introducing Interpolating Modified Moving Least Squares (IMMLS) shape functions, which improve the enforcement of essential boundary conditions and enhance approximation quality compared with traditional EFG formulations [15-17]. In addition, interpolating and improved EFG-type formulations have shown promising numerical performance for elasticity and large-deformation analysis [18, 19]. Previous studies have demonstrated the potential of IMMLS-based formulations mainly in fracture mechanics and selected deformation-related applications. However, their application to the large-deformation analysis of hyperelastic solids remains limited, especially for Neo-Hookean materials and in terms of quantitative assessment of stress-field prediction and convergence behavior. Compared with conventional MLS-based EFG approximations, the IMMLS formulation is particularly attractive for hyperelastic large-deformation problems because its near-interpolating property facilitates the imposition of essential boundary conditions while maintaining stable approximation under strong nonlinear deformation. In parallel, several alternative meshfree frameworks, including meshless local Petrov-Galerkin formulations and related approaches, have also been applied to finite-deformation and hyperelastic analyses [20-24]. In the present study, an IMMLS-based meshfree method is employed for the large-deformation analysis of hyperelastic solids governed by the Neo-Hookean material law, chosen for its simplicity and relevance to rubber-like materials [25].

## 2. Hyperelastic constitutive model

The considered material is compressible hyperelastic and modeled using the Neo-Hookean formulation. Large deformation kinematics is

expressed via the deformation gradient **F**, from which the Jacobian J=det **F** and the right Cauchy-Green tensor **C**=$\mathbf{F}^{\mathrm{T}}\mathbf{F}$ are derived. The strain energy function is given by.

$$\mathbf{W}=\frac{\mu}{2}(\mathrm{I}_1\text{-}3)\text{-}\mu\ln(\mathrm{J})+\frac{\kappa}{2}(\ln(\mathrm{J}))^2 \quad (1)$$

In which, $\mathrm{I}_1=\mathrm{tr}(\mathbf{C})$, and μ, κ are shear and bulk modulus, respectively. The first Piola-Kirchhoff stress tensor is given as

$$\mathbf{P}=\mu(\mathbf{F}-\mathbf{F}^{-\mathrm{T}})+\kappa\ln(\mathrm{J})\cdot\mathbf{F}^{-\mathrm{T}} \quad (2)$$

This formulation captures moderate to large compressible behavior in a compact form and is commonly used for soft materials like rubber or biological tissue.

## 3. Meshfree discretization and solution procedure

The Interpolating Modified Moving Least Squares (IMMLS) method can be regarded as a refined version of the conventional Moving Least Squares Approximation (MLSA), designed to improve approximation behavior while preserving numerical stability. By introducing a regularized weighting treatment, IMMLS generates near-interpolating shape functions and allows essential boundary conditions to be imposed more conveniently than in standard MLS-based formulations [17]. These properties make the method attractive for nonlinear analyses involving large deformation and hyperelastic response.

In the IMMLS framework, the value of a scalar field at a point $\mathbf{x}$ is approximated locally by a polynomial basis together with a vector of unknown coefficients. The unknown coefficients are determined through a weighted least-squares procedure carried out over the support domain associated with the evaluation point.

$$\mathrm{u}^{\mathrm{h}}(\mathbf{x})=\mathbf{p}^{\mathrm{T}}(\mathbf{x})\mathbf{a}(\mathbf{x}) \quad (3)$$

Where $\mathbf{p}(\mathbf{x})$ is the polynomial basis vector (quadratic basis $[1,\mathrm{x},\mathrm{y},\mathrm{x}^2,\mathrm{xy},\mathrm{y}^2]$ in this study), and $\mathbf{a}(\mathbf{x})$ is the unknown coefficient vector. The coefficients are obtained by minimizing the functional

$$\mathrm{J}(\mathbf{x})=\sum_{\mathrm{i}=1}^{\mathrm{n}}\mathrm{w}(\mathbf{x}-\mathbf{x}_{\mathrm{i}})\left[\mathrm{u}^{\mathrm{h}}(\mathbf{x}_{\mathrm{i}})-\mathrm{u}_{\mathrm{i}}\right]^2+\mathbf{a}^{\mathrm{T}}(\mathbf{x})\mathbf{N}\mathbf{a}(\mathbf{x}) \quad (4)$$

where $\mathrm{n}$ is the number of nodes in the support domain, $\mathrm{w}(\cdot)$ is the weight function, and $\mathbf{N}$ is a penalty matrix that stabilizes higher-order terms. The polynomial basis matrix $\mathbf{P}\in\mathbb{R}^{m\times n}$ and diagonal weight matrix $\mathbf{W}\in\mathbb{R}^{n\times n}$ are

$$\mathbf{P}=\begin{bmatrix}\mathrm{p}_1(\mathbf{x}_1) & \cdots & \mathrm{p}_1(\mathbf{x}_{\mathrm{n}})\\ \vdots & \ddots & \vdots\\ \mathrm{p}_{\mathrm{m}}(\mathbf{x}_1) & \cdots & \mathrm{p}_{\mathrm{m}}(\mathbf{x}_{\mathrm{n}})\end{bmatrix}$$
$$\mathbf{W}=\mathrm{diag}[\mathrm{w}_1(\mathbf{x}),\ldots,\mathrm{w}_{\mathrm{n}}(\mathbf{x})] \quad (5)$$

where $\mathrm{m}$ is the number of basis terms and $\mathrm{w}_{\mathrm{i}}(\mathbf{x})$ is the nodal weight.

For two-dimensional problemsm, the penalty matrix is defined as

$$\mathbf{N}=\begin{bmatrix}0_{3\times3} & 0_{3\times3}\\ 0_{3\times3} & \mathrm{diag}(\mu_{\mathrm{x}^2},\mu_{\mathrm{xy}},\mu_{\mathrm{y}^2})\end{bmatrix}_{6\times6} \quad (6)$$

where $\mu_{\mathrm{x}^2},\mu_{\mathrm{xy}},\mu_{\mathrm{y}^2}>0$ are small parameters applied to the higher-orer terms.

Minimizing Eq.(4) with respect to $\mathbf{a}(\mathbf{x})$ leads to

$$[\mathbf{P}\mathbf{W}\mathbf{P}^T+\mathbf{N}]\mathbf{a}(\mathbf{x})-\mathbf{P}\mathbf{W}\mathbf{u}=0 \quad (7)$$

with the moment and auxiliary matrices

$$\mathbf{A}(\mathbf{x})=\mathbf{P}\mathbf{W}\mathbf{P}^T+\mathbf{N}=\sum_{i=1}^{n}\mathbf{p}(\mathbf{x}_i)\,w_i(\mathbf{x})\mathbf{p}^T(\mathbf{x}_i)+\mathbf{N} \quad (8)$$

$$\mathbf{B}(\mathbf{x})=\mathbf{P}\mathbf{W}=[w_1(\mathbf{x})\mathbf{p}(\mathbf{x}_1),\ldots,w_n(\mathbf{x})\mathbf{p}(\mathbf{x}_n)] \quad (9)$$

Eliminating $\mathbf{a}(\mathbf{x})$ from Eq. (7) yields the approximation

$$\mathrm{u}^{\mathrm{h}}(\mathbf{x})=\mathbf{p}^{\mathrm{T}}(\mathbf{x})[\mathbf{P}\mathbf{W}\mathbf{P}^{\mathrm{T}}+\mathbf{N}]^{-1}\mathbf{P}\mathbf{W}\mathbf{u}=\sum_{\mathrm{i}=1}^{\mathrm{n}}\Phi_{\mathrm{i}}(\mathbf{x})\mathrm{u}_{\mathrm{i}} \quad (10)$$

Where $\mathbf{\Phi}(\mathbf{x})$represents the IMMLS shape function vector.

$$\mathbf{\Phi}(\mathbf{x})=[\Phi_1(\mathbf{x}),\ldots,\Phi_n(\mathbf{x})]=\mathbf{p}^{\mathrm{T}}(\mathbf{x})[\mathbf{P}\mathbf{W}\mathbf{P}^{\mathrm{T}}+\mathbf{N}]^{-1}\mathbf{P}\mathbf{W} \quad (11)$$

To obtain the near-interpolating condition ($\mathbf{\Phi}_i(\mathbf{x}_j) \approx \delta_{ij}$), a regularized weight function is introduced. Here, $s$ denotes the distance from the evaluation point to node $i$, $R$ is the support radius, and $\chi$ is a small regularization parameter, taken as $10^{-5}$ in the present study.

$$w_R(s) = \frac{\left[\left(\frac{s}{R}\right)^2 + \chi\right]^{-2} - (1+\chi)^{-2}}{\chi^{-2} - (1+\chi)^{-2}} \quad (12)$$

With this construction, IMMLS maintains the approximation accuracy of the classical MLSA while yielding stable shape functions for arbitrary nodal arrangements and allowing the direct enforcement of essential boundary conditions. This is particularly beneficial for nonlinear finite-strain problems, where the numerical formulation must remain robust while accommodating large deformations, sharp displacement gradients, and boundary constraints at the same time.

A Newton-Raphson iterative scheme solves

$$\mathbf{K}^{(i)}\Delta\mathbf{u}^{(i)} = \mathbf{R}^{(i)}, \quad u^{(i+1)} = \mathbf{u}^{(i)} + \Delta\mathbf{u}^{(i)} \quad (13)$$

By linearizing $\mathbf{P}$ with respect to $\mathbf{F}$, the tangent stiffness matrix $\mathbf{K}$ is established for the iterative solution process. An incremental loading procedure is adopted to enhance convergence when large strains are present. Furthermore, the meshfree character of IMMLS provides clear advantages for problems with complex geometrical configurations and pronounced deformation, since numerical difficulties related to remeshing and mesh distortion can be largely avoided.

## 4. Results and discussion

This section applies the proposed IMMLS meshfree method to two problems to demonstrate its versatility and effectiveness. The first is a benchmark rectangular plate under compression, validating the method against literature results. The second is a custom curved beam with a horizontal extension, assessing performance on complex geometries and stress concentrations. These examples illustrate the accuracy and practical advantages of the IMMLS approach.

### 4.1. Case study with rectangular plate under compression

The first problem involves a rectangular plate, aimed at verifying and comparing the method with a similar problem presented in the study by Hassani et al [25]. The problem employs a hyperelastic material modeled using the Neo-Hookean formulation, with shear modulus $\mu$ of 80.1938 $(N/mm^2)$ and bulk modulus $\kappa$ of 120.291$(N/mm^2)$ in the compressible regime. These values are obtained from experimental measurements.

#### 4.1.1. Boundary condition

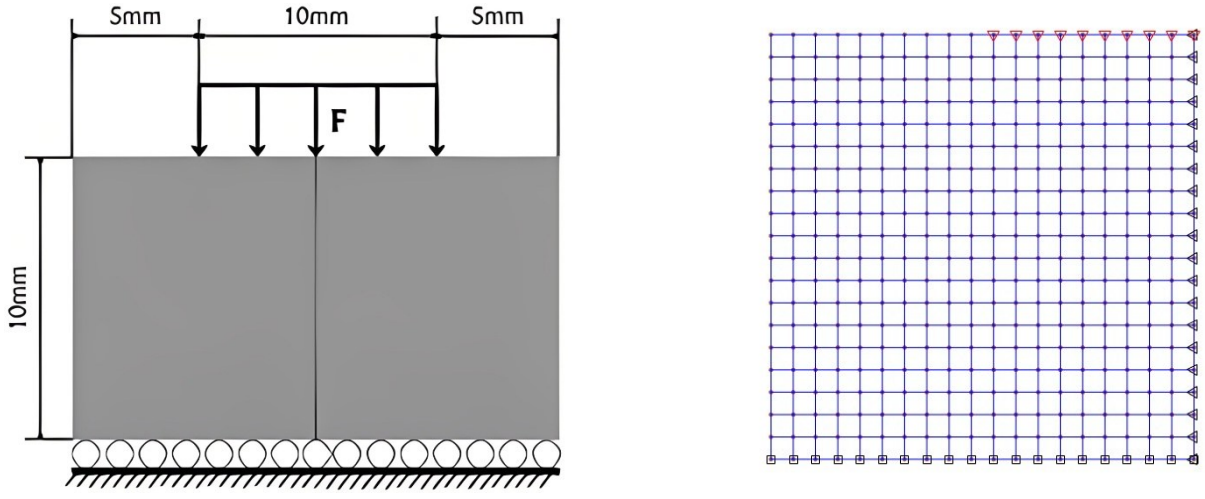


(a) (b)

**Fig. 1.** Rectangular plate under compression
(a) Schematic of rectangular plate (b) Background cells of the left half of the model

Fig. 1a illustrates the model of rectangular plate with dimensions of 20 mm × 10 mm. The bottom edge of the plate is vertically constrained, i.e. all points along this edge are fixed in vertical direction $(u_y = 0)$. A uniformly distributed load $\mathbf{F}$ is applied over the central 10 mm segment of the top edge, while two lateral edges have no constraint.

Fig. 1b shows the nodal distribution and background cells constructed for the analysis domain using the meshfree method. Nodes are uniformly distributed over the entire plate, and the nodes along the bottom edge are constrained in the y-direction to enforce the clamped boundary condition.

#### 4.1.2. Cauchy-Green stress and Piola-Kirchhoff stress

Fig. 2 illustrates the distributions of the Cauchy and first Piola-Kirchhoff stress fields for the rectangular plate under compression undergoing large deformation, as obtained by the proposed meshfree IMMLS method. In general, both sets of stress contours show smooth and continuous variation over the entire domain, indicating that the formulation is able to capture the nonlinear stress response in a stable manner. The stress fields also clearly reflect the effect of compression combined with geometric change, especially in the region where the plate bends and the deformation become more pronounced. This demonstrates that the IMMLS approximation is capable of representing not only the global deformation pattern but also the associated local stress redistribution.

Fig. 2a presents the components of the Cauchy stress tensor. It can be observed that the normal stress components, particularly $\sigma_{xx}$, $\sigma_{yy}$, exhibit strong gradients in the regions close to the loaded boundary and in the curved transition zone generated by the deformation. These regions correspond to the main load-transfer path, where compressive effects and geometric nonlinearity interact most significantly. Such a response is physically reasonable for a compressed plate undergoing large deformation, where bending and local distortion modify the internal stress distribution considerably.

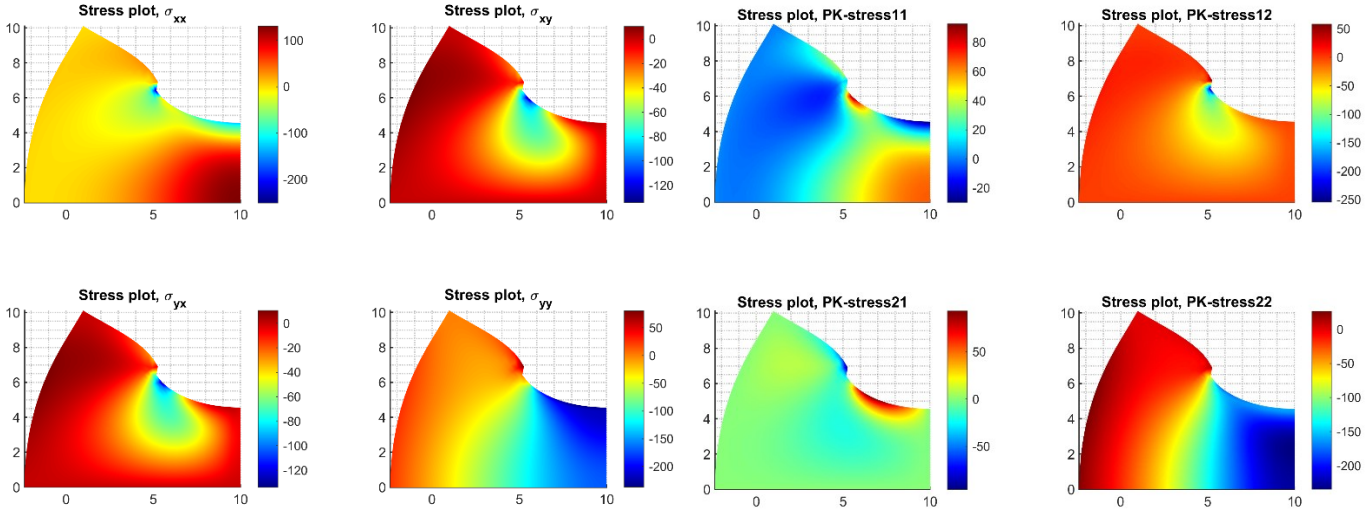


(a) (b)

**Fig. 2**. Distribution of stress fields. Cauchy-Green (a) and Piola-Kirchhoff (b) stress fields over the rectangular plate under compression

Fig. 2b shows the corresponding components of the first Piola-Kirchhoff stress tensor. In general, the spatial distribution patterns are consistent with those of the Cauchy stress field, especially regarding the location of the highly stressed regions and the overall trend of stress variation. Nevertheless, differences in magnitude and sign can be observed for several components,

which is expected because the first Piola-Kirchhoff stress is defined with respect to the reference configuration, whereas the Cauchy stress is associated with the current deformed configuration. Therefore, the two stress measures are not identical in value, but they should still describe the same physical behaviour in a consistent way. The present results satisfy this expectation, since both tensors indicate similar mechanically critical regions and comparable stress-transfer characteristics.

#### 4.1.3. Comparison and convergence study

Fig. 3 presents a convergence and validation study of the resultant displacement for the rectangular plate under compression problem, simulated using the meshfree IMMLS method. The results are compared with the reference data by Hassani et al [25].

The horizontal axis shows the number of nodes along each direction (nnx = nny), reflecting mesh refinement. The vertical axis shows the resultant displacement (mm) at the point of maximum response for different loading intensities (f = 50, 100, 150, 200 N/mm$^2$). The solid lines denote the present IMMLS results, whereas the dashed lines represent the reference values. It is observed that when the nodal density increases from 10 to 20, the resultant displacement changes noticeably, indicating that the solution is still sensitive to discretization for coarse meshes. However, as the mesh is further refined, the displacement values gradually stabilize. In particular, for $\mathrm{nnx} = \mathrm{nny} \geq 25$, the results become nearly unchanged, and the deviation from the reference data is very small, typically below about 2%.

Fig. 4 provides a quantitative evaluation of the convergence behaviour through the relative error of the resultant displacement for different nodal discretization and loading levels. It can be clearly seen that the error is relatively high for coarse nodal distributions, particularly at the smallest values of $nnx$, indicating that the solution is still sensitive to discretization in this range. However, as the nodal density increases, the relative error decreases rapidly for all loading cases, showing that the numerical solution progressively approaches the reference result. For medium and fine discretizations, the error becomes very small and tends to stabilize near zero, which confirms that the displacement response has reached a converged state.

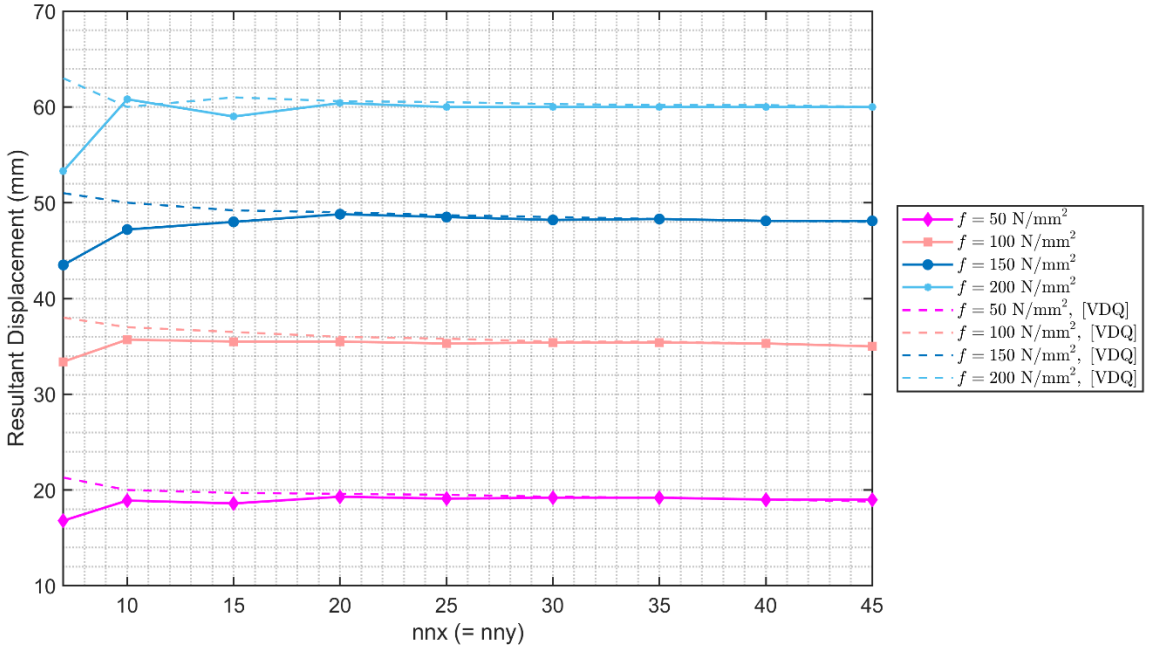


**Fig. 3.** Displacement comparison by the number of nodes on rectangular plate under compression

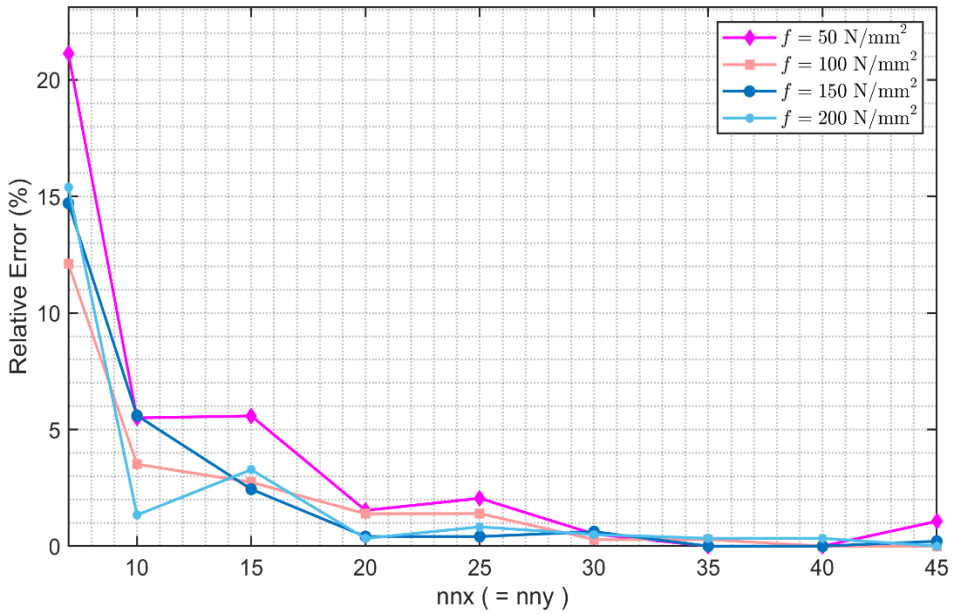


**Fig. 4.** Relative error of resultant displacement for the rectangular plate under compression

Another important observation is that the same overall trend is maintained for all applied loads, although slight differences can still be seen at coarse discretization levels. In particular, the lower load case shows a somewhat larger initial error, whereas the higher load cases tend to approach the converged range more quickly after refinement. Despite these differences, all curves eventually collapse to very small error values as the mesh is refined. This behavior is fully consistent with the convergence trend observed in Fig. 3 and confirms that the present IMMLS formulation can provide accurate and stable predictions for the large-deformation response of the rectangular plate under compression.

### 4.2. Case study with curved beam and horizontal extension under traction

The second benchmark problem, named the "Curved beam and horizontal extension under traction," features a complex geometry that combines both curved and straight segments. Similar to the previous problem, this problem also uses a hyperelastic material modeled using the Neo-Hookean formulation, with shear modulus $\mu$ of 80.1938 $(\mathrm{N/mm^2})$ and bulk modulus $\kappa$ of 120.291$(\mathrm{N/mm^2})$.

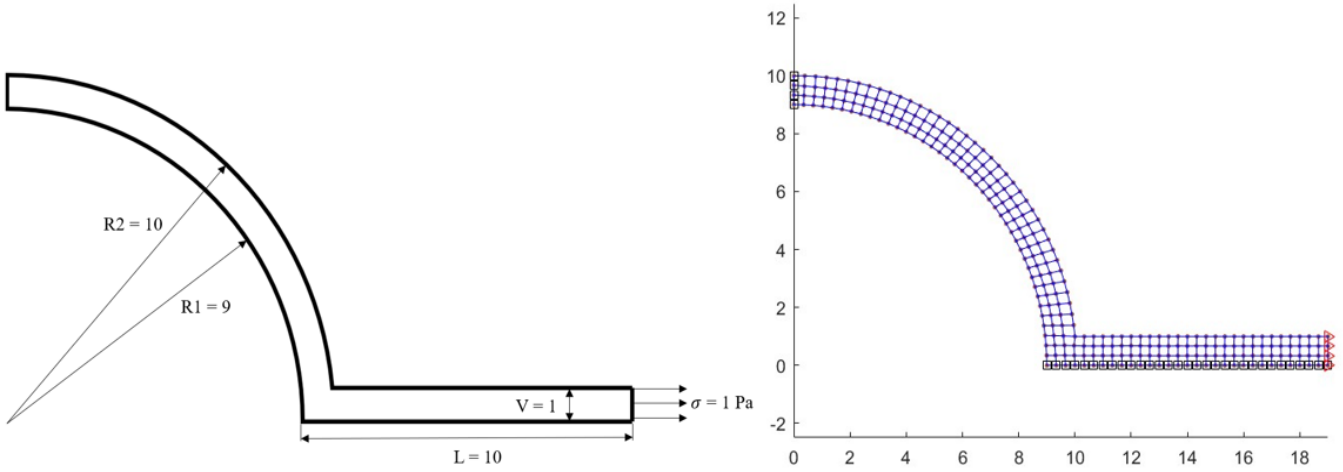


(a) (b)

**Fig. 5.** Curved beam and horizontal extension under traction (a) Schematic of curved beam and horizontal extension under traction (b) Background cells

#### 4.2.1. Boundary condition

Fig. 5 shows the geometry and meshfree node distribution for curved beam with a horizontal extension under traction, where nodes are arranged in a regular pattern to ensure sufficient resolution in both curved and straight sections. The model consists of a quarter-annular beam with an inner radius of $R_1 = 9\,m$ and an outer radius of $R_2 = 10\,m$, which is seamlessly connected to a straight rectangular extension measuring $L = 10\,m$ in length and $V = 1\,m$ in height. For boundary conditions, the left edge of the curved beam is completely fixed, i.e. displacement components at this edge are set to zero. On the opposite side, the right edge of the straight extension is subjected to a uniform tensile stress of $\sigma = 1\,Pa$ applied in the longitudinal (horizontal) direction. Nodes along the left edge are fully constrained to represent the fixed support, nodes at the right end of the horizontal extension receive the prescribed tensile traction, and all other nodes remain free, accurately representing the intended boundary conditions.

#### 4.2.2. Cauchy-Green stress and Piola-Kirchhoff stress

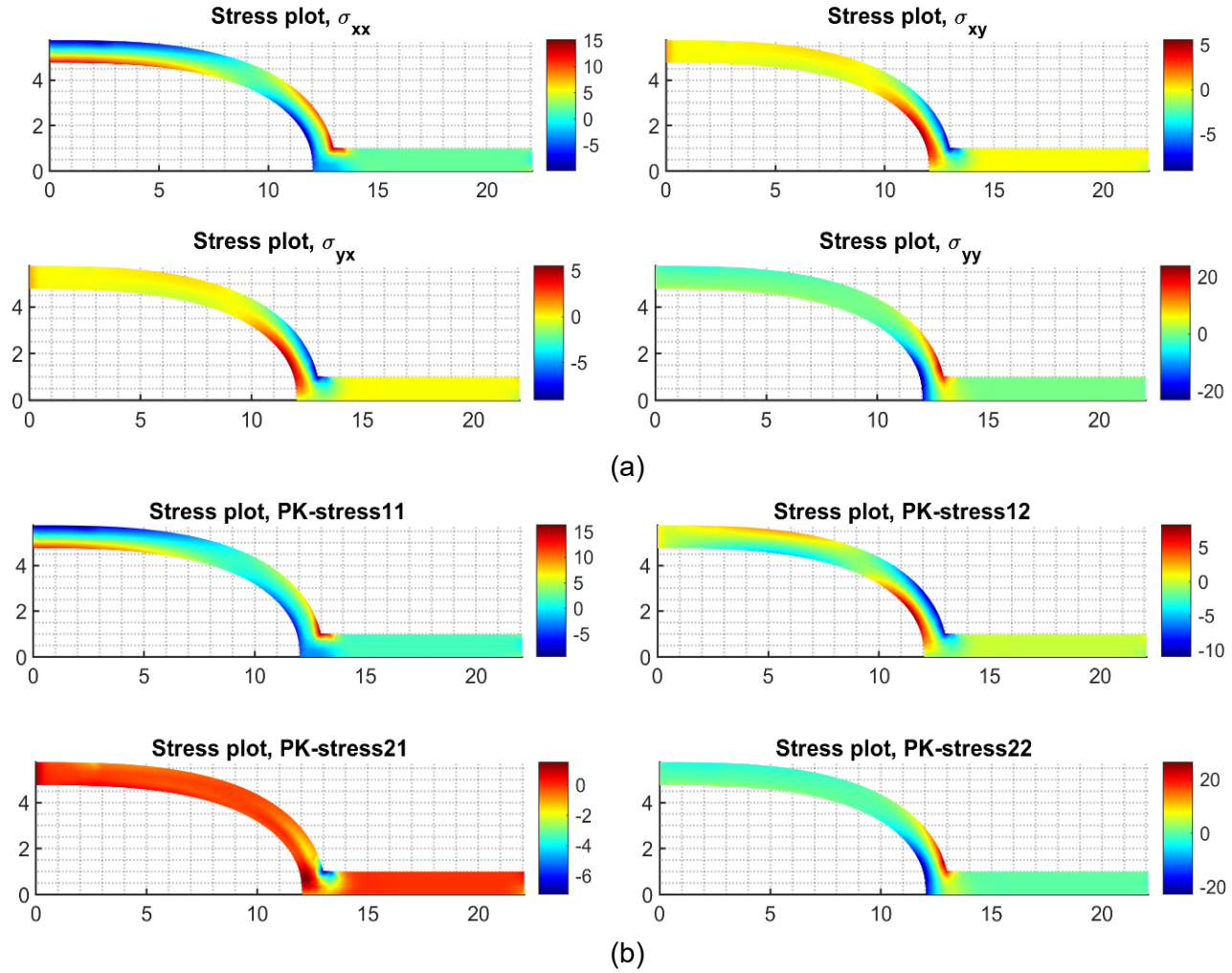


**Fig. 6.** Distribution of stress fields. Cauchy-Green (a) and Piola-Kirchhoff (b) stress fields of curved beam with horizontal extension under traction

Fig. 6 presents the distributions of the Cauchy and first Piola-Kirchhoff stress fields obtained for the curved beam with horizontal extension under traction using the proposed meshfree IMMLS formulation. Overall, both groups of stress contours exhibit smooth spatial variation along the curved geometry, without visible numerical oscillation or spurious irregularities. This indicates that the proposed approximation is able to capture the stress transfer in a geometrically

complex domain in a stable manner, even under large deformation conditions. The stress fields also clearly reflect the influence of the curved-to-straight transition region, which acts as the most critical zone in the structure due to the abrupt change in geometry and the associated redistribution of internal forces. Fig. 6a shows the components of the Cauchy stress tensor. It can be observed that the normal stress components, especially $\sigma_{xx}$, $\sigma_{yy}$ develop pronounced gradients near the transition between the curved segment and the straight extension. This region experiences the highest stress concentration because the load path changes significantly there, causing a nonuniform stress redistribution. The smoothness and continuity of the contours further demonstrate that the IMMLS approximation can represent stress fields effectively without introducing noticeable numerical noise. Fig. 6b presents the corresponding components of the first Piola-Kirchhoff stress tensor. In general, the overall distribution patterns are consistent with those observed in the Cauchy stress field, particularly in terms of the location of high-stress regions and the global variation trend along the beam. The main difference lies in the magnitude and sign of some components, which is expected because the first Piola-Kirchhoff stress is defined with respect to the reference configuration, whereas the Cauchy stress is defined in the current deformed configuration. Therefore, although the two stress measures describe the same mechanical response, they do not coincide quantitatively. Even so, both stress tensors consistently identify the transition zone as the mechanically critical region, which supports the physical reliability of the numerical solution.

#### 4.2.3. Convergence study

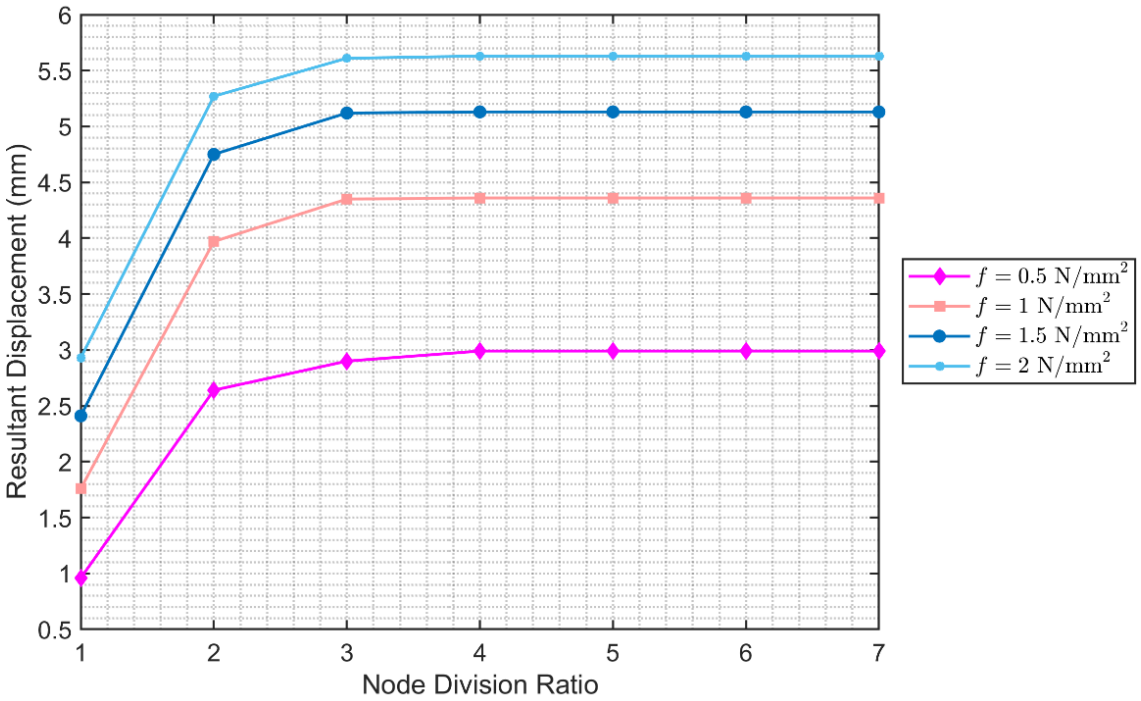


**Fig. 7.** Displacement comparison of curved beam with horizontal extension under traction

Fig. 7 presents the convergence study of the meshfree IMMLS method for the curved beam with horizontal extension under traction. The plot shows the resultant displacement at the point of maximum response as a function of the node division ratio (i.e., node density), for various levels of applied tensile load $(\mathrm{f} = 0.5, 1, 1.5, \text{and } 2\ \mathrm{N/mm^2})$. When the node division ratio increases from 1 to 3, the resultant displacement changes significantly, especially for higher loading levels. However, starting from the node division ratio of 4, displacement curves for all loading cases begin to

plateau and show negligible variation with further increases in node density. This indicates that the solution starts to converge and stabilize at a node division ratio of 4. For even finer discretization (ratios 5, 6, 7), the convergence error becomes extremely small, confirming that the IMMLS method achieves high accuracy with only a moderate node density, saving substantial computational cost compared to traditional mesh-based methods.

Fig. 8 further quantifies the convergence behavior by presenting the successive relative change in the resultant displacement between two consecutive nodal refinements under different loading levels. A clear and consistent trend can be observed for all cases: the relative change decreases markedly as the node division ratio increases, confirming that the numerical solution gradually approaches a mesh-independent state. At the coarser discretization level, especially in the transition from the ratio of 3 to 4, the variation remains relatively significant, indicating that the approximation is still sensitive to the nodal density and the response has not yet fully stabilized. This is expected because, with a limited number of nodes, the meshfree approximation still cannot capture the deformation field with sufficient accuracy. As the node division ratio increases further, the successive relative change drops rapidly for every loading case. In particular, from the ratio of 4 to 5, the reduction becomes very pronounced, and from the ratio of 5 onward the relative change is nearly zero. This means that additional nodal refinement produces only a negligible difference in the resultant displacement, which is a strong indication that the solution has already entered a stable convergence regime. Therefore, Fig. 8 does not only confirm convergence qualitatively, but also provides a quantitative measure showing that the displacement response becomes practically unchanged beyond a certain nodal density.

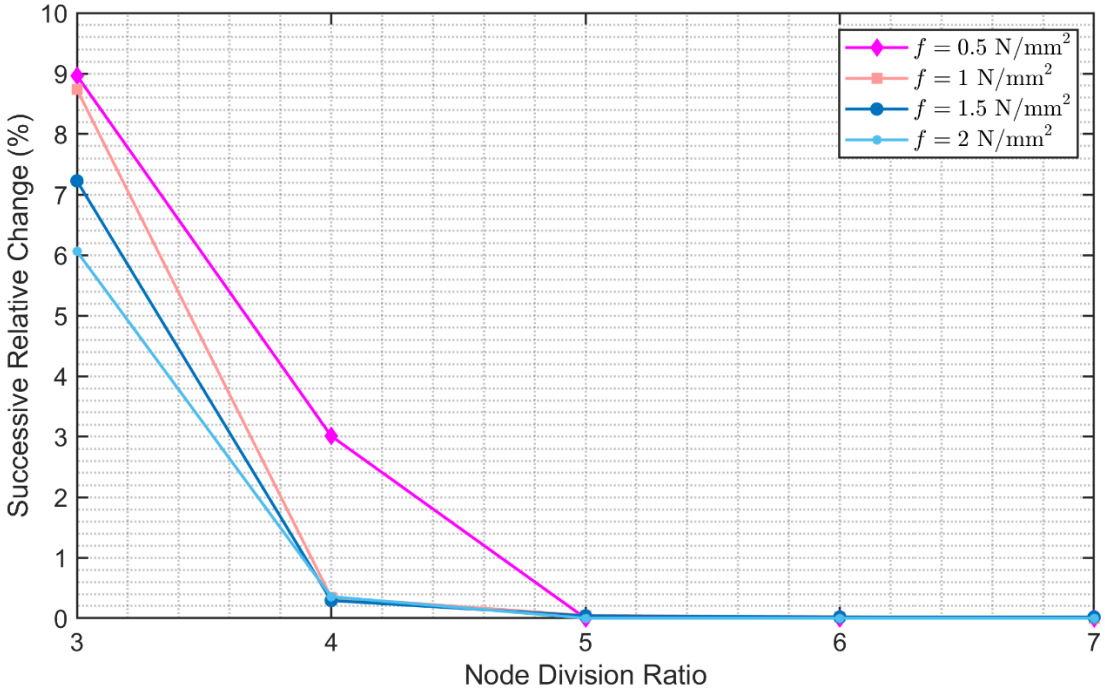


**Fig. 8.** Successive relative change of resultant displacement for the curved beam under traction

This rapid and robust convergence demonstrates the reliability of the IMMLS approach for nonlinear, large-deformation, and complex geometry problems, while highlighting its potential for efficient application in practical engineering models. The advantages of meshfree methods for large deformation hyperelastic problems have been reported in previous studies [7, 15], showing

comparable computational time to FEM with improved robustness. In this context, the present IMMLS formulation adds further benefit through its interpolation property, which allows direct enforcement of boundary conditions.

## 5. Conclusion

This study has presented and evaluated a meshfree computational framework based on the Interpolating Modified Moving Least Squares (IMMLS) approximation for hyperelastic materials subjected to large deformation. The method was applied to both classical benchmark problem (i.e. the rectangular plate under compression) and custom complex geometry (i.e. the curved beam with horizontal extension).

The results show that the meshfree IMMLS method is capable of accurately simulating the distribution of Cauchy-Green and Piola-Kirchhoff stresses, feasible in handling those problems under conditions of significant deformation and nonlinearity. The method yields smooth, stable, noise-free stress fields, clearly representing zones of stress concentration and nonlinear phenomena in agreement with theory and reference solutions. Convergence studies confirm that the IMMLS method achieves stable and rapid convergence with only moderate node densities. For both problems, the solution becomes stable and accurate after surpassing a certain node division threshold, demonstrating higher efficiency and reliability compared to traditional mesh-based approaches. Notably, the method does not exhibit “locking” or mesh-dependency, which are often encountered in finite element methods (FEM) for large-deformation hyperelastic analysis.

Key advantages include the requirement for mesh generation, suitability for complex geometries and materials, robust interpolation, and high computational efficiency. However, the choice and optimization of weight functions, handling complex boundary conditions, and computational cost for large-scale 3D problems remain challenges. Future work should address improving boundary condition enforcement, extending the method to 3D and more complex materials, and optimizing for parallel computing. IMMLS also holds promise for coupled multi-physics and gradient material models.

## Acknowledgments

We acknowledge Ho Chi Minh City University of Technology (HCMUT), VNU-HCM and The University of Queensland (UQ) for supporting this study.

## References

[1] H.B. Khaniki, M.H. Ghayesh, R. Chin, M. Amabili. (2023). Hyperelastic structures: A review on the mechanics and biomechanics. *International Journal of Non-Linear Mechanics*, 148, 104275. https://doi.org/10.1016/j.ijnonlinmec.2022.104275

[2] J. Dolbow, T. Belytschko. (1999). Volumetric locking in the element free Galerkin method. *International Journal for Numerical Methods in Engineering*, 46(6), 925-942. https://doi.org/10.1002/(SICI)1097-0207(19991030)46:6%3C925::AID-NME729%3E3.0.CO;2-Y

[3] S.S. Kumar, A. Shaji, N. Muthu. (2025). A two-field mixed formulation with scattered pressure node distribution in element-free Galerkin method for alleviating volumetric locking in hyperelastic materials. *Acta Mechanica Sinica*, 41, 424446. https://doi.org/10.1007/s10409-024-24446-x

[4] R. Rossi, M.K. Alves. (2007). On the Analysis of an EFG Method Under Large Deformations and Volumetric Locking. *Computational Mechanics*, 39(4), 381-399. https://doi.org/10.1007/s00466-006-0035-z

[5] G. Bourantas, B.F. Zwick, G.R. Joldes, A. Wittek, K. Miller. (2021). Simple and robust element-free Galerkin method with almost interpolating shape functions for finite deformation elasticity. *Applied Mathematical*

*Modelling*, 96, 284-303. https://doi.org/10.1016/j.apm.2021.03.007

[6] T. Belytschko, Y.Y. Lu, L. Gu. (1994). Element-free Galerkin methods. *International Journal for Numerical Methods in Engineering*, 37(2), 229-256. https://doi.org/10.1002/nme.1620370205

[7] E. Khosrowpour, M.R. Hematiyan, M. Hajhashemkhani. (2019). A strong-form meshfree method for stress analysis of hyperelastic materials. *Engineering Analysis with Boundary Elements*, 109, 32-42. https://doi.org/10.1016/j.enganabound.2019.09.013

[8] S. Cai, D.M. Li, J.-x. Xie. (2023). A complex variable EFG method for hyperelastic large deformation analysis under non-conservative loads. *Applied Mathematical Modelling*, 113, 596-612. https://doi.org/10.1016/j.apm.2022.09.024

[9] J.-S. Chen, C. Pan, C.-T. Wu, W.K. Liu. (1996). Reproducing Kernel Particle Methods for large deformation analysis of non-linear structures. *Computer Methods in Applied Mechanics and Engineering*, 139(1-4), 195-227. https://doi.org/10.1016/S0045-7825(96)01083-3

[10] S. Jun, W.K. Liu, T. Belytschko. (1998). Explicit Reproducing Kernel Particle Methods for large deformation problems. *International Journal for Numerical Methods in Engineering*, 41(1), 137-166. https://doi.org/10.1002/(SICI)1097-0207(19980115)41:1%3C137::AID-NME280%3E3.0.CO;2-A

[11] S. Li, W. Hao, W.K. Liu. (2000). Numerical simulations of large deformation of thin shell structures using meshfree methods. *Computational Mechanics*, 25, 102-116. https://doi.org/10.1007/s004660050463

[12] J.-S. Chen, C.-T. Wu, S. Yoon, Y. You. (2001). A stabilized conforming nodal integration for Galerkin mesh-free methods. *International Journal for Numerical Methods in Engineering*, 50(2), 435-466. https://doi.org/10.1002/1097-0207(20010120)50:2%3C435::AID-NME32%3E3.0.CO;2-A

[13] J.-S. Chen, M. Hillman, S.-W. Chi. (2017). Meshfree Methods: Progress Made after 20 Years. *Journal of Engineering Mechanics*, 143(4), 04017001. https://doi.org/10.1061/(ASCE)EM.1943-7889.0001176

[14] A. Huerta, S. Fernández-Méndez. (2001). Locking in the incompressible limit for the element-free Galerkin method. *International Journal for Numerical Methods in Engineering*, 51(11), 1361-1383. https://doi.org/10.1002/nme.213

[15] N.T. Nguyen, M.N. Nguyen, T.T. Truong, T.Q. Bui. (2021). An improved meshless method for finite deformation problem in compressible hyperelastic media. *Vietnam Journal of Mechanics*, 43(1), 27-41. https://doi.org/10.15625/0866-7136/15332

[16] T.V. Vu, N.T. Nguyen, M.N. Nguyen, T.T. Truong, T.Q. Bui. (2021). A Meshfree Method Based on Integrated Radial Basis Functions for 2D Hyperelastic Bodies. *Modern Mechanics and Applications, pp. 990-1003.* https://doi.org/10.1007/978-981-16-3239-6_78

[17] S.K. Lohit, A.K. Gaonkar, T.P. Gotkhindi. (2022). Interpolating Modified Moving Least Squares based element free Galerkin method for fracture mechanics problems. *Theoretical and Applied Fracture Mechanics*, 122, 103569. https://doi.org/10.1016/j.tafmec.2022.103569

[18] Q. Wu, P. Peng, Y. Cheng. (2021). The interpolating element-free Galerkin method for elastic large deformation problems. *Science China Technological Sciences*, 64, 364-374. https://doi.org/10.1007/s11431-019-1583-y

[19] F. Liu, Y. Cheng. (2018). The Improved Element-Free Galerkin Method Based on the Nonsingular Weight Functions for Elastic Large Deformation Problems. *International Journal of Computational Materials Science and Engineering*, 7(4), 1850023.

https://doi.org/10.1142/S2047684118500239

[20] D. Hu, Z. Sun, C. Liang, X. Han. (2013). A mesh-free algorithm for dynamic impact analysis of hyperelasticity. *Acta Mechanica Solida Sinica*, 26(4), 362-372. https://doi.org/10.1016/S0894-9166(13)60033-6

[21] D. Hu, Z. Sun. (2011). The Meshless Local Petrov-Galerkin Method for Large Deformation Analysis of Hyperelastic Materials. *International Scholarly Research Notices*, 2011, 967512. https://doi.org/10.5402/2011/967512

[22] D.A. Hu, S.Y. Long, X. Han, G.Y. Li. (2007). A meshless local Petrov–Galerkin method for large deformation contact analysis of elastomers. *Engineering Analysis with Boundary Elements*, 31(7), 657-666. https://doi.org/10.1016/j.enganabound.2006.11.005

[23] B. Calvo, M.A. Martinez, M. Doblaré. (2005). On solving large strain hyperelastic problems with the natural element method. *International Journal for Numerical Methods in Engineering*, 62(2), 159-185. https://doi.org/10.1002/nme.1164

[24] W.-L. Fan, X.-W. Gao, F. Peng, B.-B. Xu. (2025). A total Lagrangian Galerkin free element method for finite deformation in hyperelastic materials. *Applied Mathematical Modelling*, 137(Part B), 115740. https://doi.org/10.1016/j.apm.2024.115740

[25] R. Hassani, R. Ansari, H. Rouhi. (2019). Large deformation analysis of 2D hyperelastic bodies based on the compressible nonlinear elasticity: A numerical variational method. *International Journal of Non-Linear Mechanics*, 116, 39-54. https://doi.org/10.1016/j.ijnonlinmec.2019.05.003